 ©2020 Kvantovaya Elektronika and Turpion Ltd

https://doi.org/10.1070/QEL17137

Two-dimensional image edge enhancement using two orders of Bragg diffraction

V.M. Kotov, S.V. Averin

Abstract. **The process of two-dimensional image edge enhancement with an acousto-optical spatial filter using two orders of light diffraction is studied. It is theoretically shown that the diffraction that occurs in a paratellurite crystal on a 'slow' acoustic wave propagating orthogonally to the optical axis of the crystal allows enhancing a two-dimensional edge of an image, transferred by optical radiation with a wavelength of 0.63 μm in a wide band of acoustic frequencies 25–50 MHz. Enhancement of a two-dimensional image edge at an acoustic frequency of 29 MHz is experimentally demonstrated.**

Keywords: *two-dimensional image edge enhancement, acousto-optical diffraction, Bragg diffraction, two-order diffraction.*

1. Introduction

Acousto-optical (AO) interaction is an efficient method for controlling the parameters of not only an individual optical beam, but also a set of beams carrying an image [1–4]. One of the widely used methods of image processing is the edge enhancement. The edge (contour), being only a small part of the image, contains information about such important characteristics of the object as its shape and size, spatial orientation, velocity and character of motion, etc.

For edge enhancement, optical Fourier processing of the image is most widely used, where the AO cell serves as a spatial frequency filter [5]. While at first AO cells were used for filtering one-dimensional images (see, e.g., [6–8]), it was subsequently found that they can be successfully used for processing two-dimensional images, in particular, for two-dimensional edge enhancement. This is possible using special cuts of crystals or choosing special modes of AO diffraction [9–15].

One of the important characteristics of AO cells used as spatial frequency filters is the spatial frequency passband, which, in fact, determines the ultimate resolution of the cell [5]. To increase the ultimate resolution of the cell, ceteris paribus, it is necessary to reduce the frequency of the acoustic wave [5]. Note that AO filters based on quasi-collinear diffraction in TeO_2 and designed to process radiation with a wavelength of 0.63 μm operate at an acoustic frequency of 98 MHz [16], and filters with tangential geometry operate at 68 MHz [9]. It was possible to achieve a significant decrease in the acoustic frequency by using the multiple diffraction regime [12–15]; in this case, the acoustic frequency decreased to ~35 MHz for the twofold regime, and to 27 MHz for the threefold regime. However, multiple regimes are realised with significant consumption of acoustic power.

In this work, to enhance the two-dimensional image edge, we use an AO cell with two orders of diffraction. This regime is the most economical in terms of controlling power consumption: for example, to obtain 100% diffraction efficiency, the required power is half the power for the 'common' Bragg regime and one-fourth the power for the double diffraction regime [1]. In other words, the proposed regime can significantly reduce the power consumption required to control the AO cell during image processing. In addition, as will be shown below, the filters under consideration provide two-dimensional edge enhancement in a wide band of acoustic frequencies.

2. Theory

Figure 1 shows a diagram of the AO interaction that underlies the proposed regime. The beam of optical radiation denoted by P_0 and containing information about the image, propagates approximately along the optical axis z of the uniaxial gyrotropic crystal, which can be a TeO_2 (paratellurite) crystal. Orthogonal to the z axis, an acoustic wave propagates with the wave vector $\boldsymbol{K}$. As a result of the AO interaction, the incident radiation diffracts in the directions of diffraction orders +1 (beam P_{+1}) and –1 (beam P_{-1}). Image processing uses the zero Bragg order.

In determining the transfer functions, we assume that the optical field is a set of plane waves, the diffraction of these plane waves occurring independently. The waves interact with a plane monochromatic acoustic wave; therefore, the dif-

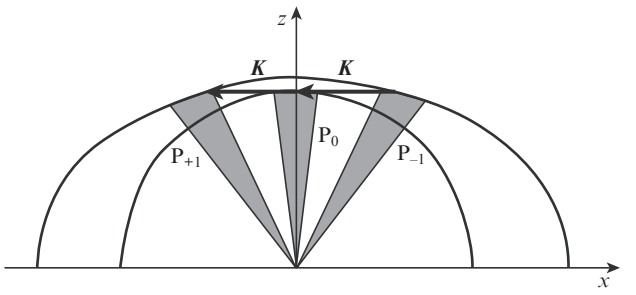

Figure 1. Diagram of AO diffraction in two orders.

V.M. Kotov, S.V. Averin Kotelnikov Institute of Radio Engineering and Electronics (Fryazino Branch), Russian Academy of Sciences, pl. Akad. Vvedenskogo 1, 141190 Fryazino, Moscow region, Russia; e-mail: vmk277@ire216.msk.su

Received 23 October 2019; revision received 30 December 2019
Kvantovaya Elektronika **50** (3) 305–308 (2020)
Translated by V.L. Derbov

fracted field is also a set of plane waves. We write the wave amplitudes for diffraction orders in the form

$$E_0(\theta_m) = E_{\text{inc}}(\theta_m)H_0(\theta_m),\ E_1(\theta_m + K/k) = E_{\text{inc}}(\theta_m)H_1(\theta_m),$$
$$E_{-1}(\theta_m - K/k) = E_{\text{inc}}(\theta_m)H_{-1}(\theta_m). \quad (1)$$

Here, E_0, E_1 and E_{-1} are the field amplitudes for the diffraction orders 0, +1, and –1, respectively; E_{inc} is the field amplitude of incident radiation; θ_m is the angle of orientation of the plane wave relative to the direction of propagation of radiation; m is the plane wave number; K and k are the wave vector magnitudes for the acoustic and optical plane waves, respectively; and H_0, H_1 and H_{-1} are the transfer functions for the diffraction orders 0, +1, and –1, respectively. These functions are related by the system of differential equations [1]:

$$\frac{dH_0}{dz} = -\frac{v}{2}[H_1\exp(-i\eta_1 z) + H_{-1}\exp(-i\eta_2 z)],$$
$$\frac{dH_1}{dz} = \frac{v}{2}H_0\exp(i\eta_1 z), \quad (2)$$
$$\frac{dH_{-1}}{dz} = \frac{v}{2}H_0\exp(i\eta_2 z).$$

Here $v = (\pi/\lambda)\sqrt{M_2 P_{\text{ac}}/(Lh)}$ is the parameter associated with the power of the acoustic wave: is the wavelength of light; M_2 is the parameter characterising AO quality of the material; L is the length of the AO interaction; h is the height of the acoustic column; P_{ac} is the acoustic power; z is the coordinate along which AO interaction develops; $\eta_1 = k_z - k_{z(+1)}$ and $\eta_2 = k_z - k_{z(-1)}$ are the phase-matching detunings for the diffraction orders +1 and –1, respectively; and k_z, $k_{z(+1)}$, $k_{z(-1)}$ are the z-components of the wave vectors for the diffraction orders 0, +1, and –1, respectively.

For the boundary conditions $H_0 = 1$ and $H_1 = H_{-1} = 0$ at $z = 0$, the solution of system (2) has the form

$$H_0 = a_1\exp(i\beta_1 z) + a_2\exp(i\beta_2 z) + a_3\exp(i\beta_3 z),$$
$$H_1 = \frac{v}{2i}\left\{\frac{a_1}{\beta_1+\eta_1}\exp[i(\beta_1+\eta_1)z] + \frac{a_2}{\beta_2+\eta_1}\exp[i(\beta_2+\eta_1)z] + \frac{a_3}{\beta_3+\eta_1}\exp[i(\beta_3+\eta_1)z]\right\}, \quad (3)$$
$$H_{-1} = \frac{v}{2i}\left\{\frac{a_1}{\beta_1+\eta_2}\exp[i(\beta_1+\eta_2)z] + \frac{a_2}{\beta_2+\eta_2}\exp[i(\beta_2+\eta_2)z] + \frac{a_3}{\beta_3+\eta_2}\exp[i(\beta_3+\eta_2)z]\right\}.$$

Here

$$a_1 = \frac{T_1}{T_1+T_2+T_3};\ a_2 = \frac{T_2}{T_1+T_2+T_3};\ a_3 = \frac{T_3}{T_1+T_2+T_3}; \quad (4)$$

$$T_1 = (\beta_3-\beta_2)(\beta_1+\eta_1)(\beta_1+\eta_2);\ T_2 = (\beta_1-\beta_3)(\beta_2+\eta_1)(\beta_2+\eta_2);$$
$$T_3 = (\beta_2-\beta_1)(\beta_3+\eta_1)(\beta_3+\eta_2);$$

and $\beta_1, \beta_2, \beta_3$ are the roots of the cubic equation

$$\beta^3 + \beta^2(\eta_1+\eta_2) + \beta(\eta_1\eta_2 - 0.5v^2) - 0.25v^2(\eta_1+\eta_2) = 0. \quad (5)$$

The two-dimensionality of the transfer functions, i.e., their dependence on the coordinate along the y axis, orthogonal to the x and z axes, was taken into account as follows. The refractive indices $n_{1,2}$ for the optical waves in the uniaxial TeO_2 crystal were expressed in the form of three-dimensional distributions [17]

$$n_{1,2}^2 = \frac{1+\tan^2\varphi}{\frac{1}{n_0^2} + \frac{\tan^2\varphi}{2}\left(\frac{1}{n_o^2}+\frac{1}{n_e^2}\right) \pm \frac{1}{2}\sqrt{\tan^4\varphi\left(\frac{1}{n_o^2}-\frac{1}{n_e^2}\right)^2 + 4G_{33}^2}}, \quad (6)$$

where n_o, n_e are the principal refractive indices of the crystal; φ is the angle between the optical axis of the crystal and the wave vector of the light wave; and G_{33} is the component of the gyration pseudotensor. In our case, it was assumed that anisotropic diffraction of the light wave by the acoustic wave occurs, the signs plus and minus in Eqn (6) corresponding to the incident and diffracted radiation. Three-dimensional surfaces formed by wave vectors are described by the functions $2\pi n_1/\lambda$ and $2\pi n_2/\lambda$. The diffraction plane intersects the wave surfaces; it passes through the origin and contains the acoustic wave vector $\boldsymbol{K}$. The detuning values η_1 and η_2 were determined by changing the angle of inclination of the diffraction plane to the optical axis z, and then, according to Eqns (2)–(5), the transfer functions H_0, H_1 and H_{-1} were determined.

For calculations, we used the parameters corresponding to the radiation of a He–Ne laser propagating in a TeO_2 single crystal: $\lambda = 0.63$ μm, $n_o = 2.26$, $n_e = 2.41$, $G_{33} = 2.62\times10^{-5}$, $M_2 = 1200\times10^{-18}$ s^3 g^{-1}, and the velocity of sound $V = 0.617\times10^5$ cm s^{-1} [18, 19]. In addition, it was assumed that $P_{\text{ac}} = 0.05$ W, $L = h = 0.2$ cm.

Figure 2 presents the squares of the moduli of the transfer functions, $H_0\times H_0^*$, calculated for acoustic frequencies of 25 and 50 MHz. The obtained transfer function distributions were used to extract a two-dimensional image contour by computer processing using fast Fourier transform (FFT) [20]. It can be seen that the distributions are very heterogeneous, the behaviour of functions being characterised by 'kinks'. The presence of kinks imparts a certain two-dimensionality to the distribution regions. Such distributions are characteristic of AO filters of two-dimensional images based on the addition of several optical fields (see, e.g., [21–23]). Note that such

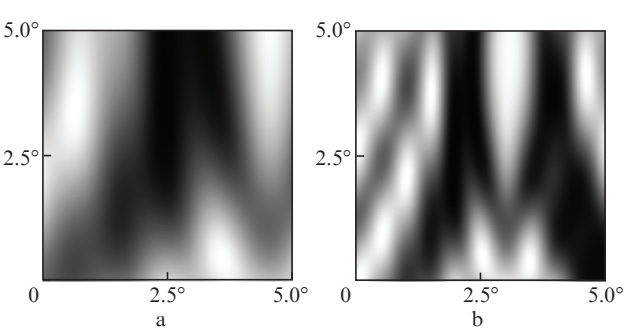

Figure 2. Transfer functions for the zero Bragg order obtained at acoustic frequencies of (a) 25 and (b) 50 MHz.

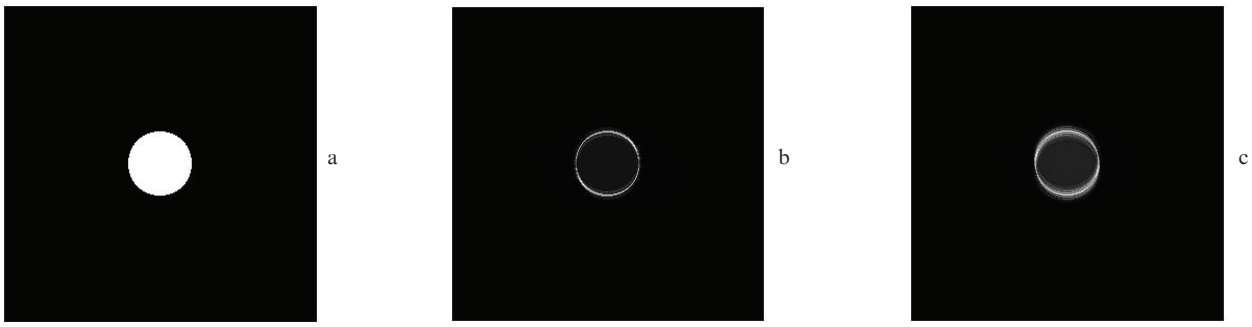

Figure 3. (a) Original image and (b, c) its appearance after FFT processing using the transfer functions obtained at frequencies of (b) 25 and (c) 50 MHz.

areas are not unique in all distributions of transfer functions. However, in the course of checking all such areas by FFT processing of two-dimensional images, the best results, based on a comparison of the contrast of the contours and their equivalence in mutually orthogonal directions, were achieved using precisely the areas shown in Fig. 2. Note that these areas correspond to the same region of the distribution of the transfer functions, but were obtained at different frequencies. In Fig. 2b the characteristic inhomogeneous regions are significantly smaller than those in Fig. 2a.

Figure 3 shows the image before processing, which is a disk (Fig. 3a), and the result of its FFT processing using the transfer functions shown in Figs 2a and 2b (Figs 3b and 3c, respectively). In Figs 3b and 3c, the contour of the disk edge is quite clearly expressed. Moreover, the edge thickness in Fig. 3b is significantly smaller than that in Fig. 3c, which is in full agreement with the results of Ref. [5]. It clearly follows that for better edge enhancement, it is necessary to use the lowest possible acoustic frequencies. However, a decrease in the acoustic frequency facilitates the transfer of light energy to higher diffraction orders, i.e., the transition to the Raman–Nath diffraction regime. In fact, the frequency of ~25 MHz is close to the minimum frequency for the Bragg diffraction regime. Indeed, the Klein–Cook parameter $Q = K^2L/k = 2\pi f^2\lambda L/V^2$ [1, 2] determines the boundary acoustic frequency f from the condition $Q \geqslant 4\pi$. For frequencies exceeding 50 MHz, the edge begins to 'blur', that is, its characteristics deteriorate significantly.

Moreover, the upper frequency value is limited by the condition for the existence of two orders of diffraction. Theoretical analysis shows that if light propagates strictly along the optical axis z, then under the condition $L\eta_{1,2} \geqslant 4$, the efficiency of diffraction in two orders does not exceed 5% [1]. In our case, the above condition restricts the upper value of the acoustic frequency to ~50 MHz.

When the incident radiation beam deviates from the z axis, the efficiency increases in one diffraction order and decreases in the other. In fact, single-order diffraction is implemented. In Ref. [24], all cases of edge enhancement using single-order Bragg diffraction were analysed. It was shown there that, except a few cases of AO interaction, diffraction into a single Bragg order does not provide the formation of a two-dimensional image contour.

3. Experiment and discussion of results

An experiment was performed to verify the above conclusions. The optical scheme of the experimental setup is described in detail in Ref. [8], where the classical method of optical Fourier image processing using two identical lenses, one for input and the other for output, is considered. The focal length of the lenses F was 18 cm. A beam of linearly polarised optical radiation with a wavelength of 0.63 μm generated by a He–Ne laser was broadened by an expander and directed to the elliptic-shaped aperture with a characteristic size of ~0.1 cm. The radiation passing through the aperture formed the initial image. The input lens was located at a distance F from the aperture in the direction of radiation propagation. A quarter-wave plate was placed between the lens and the aperture to make the radiation circularly polarised. Thus, an optical eigenwave of the TeO_2 crystal was formed, which ensured the possibility of achieving 100% diffraction efficiency. The output lens was located at a distance of $2F$ from the input lens.

Exactly in the middle between the lenses, the AO cell was located, which served as a spatial frequency filter. The AO cell was made of a TeO_2 single crystal with dimensions of 1.0, 0.8, and 0.8 cm along the [110], [1$\bar{1}$0] , and [001] directions, respectively. A transducer made of $LiNbO_3$ was glued to the {110} crystal face, generating a transverse acoustic wave with a shift along the [1$\bar{1}$0] direction. The transducer had a size of 0.2×0.2 cm and a 3 dB bandwidth of 27–40 MHz. The transducer excited a travelling acoustic wave in the crystal. The velocity of sound in the crystal was $V = 617$ m s^{-1}. Optical radiation propagated approximately along the optical axis of the crystal, passed through the output lens, and was directed to a screen located on the other side of the lens at a distance F. The image after Fourier processing, which was recorded by the camera, was observed on the screen. In the experiment, an acoustic frequency of 29 MHz was used, which is close to the minimum frequency in the frequency band of the transducer. By adjusting the AO cell (its orientation and electric power supplied to the transducer), a situation was ensured in which a two-dimensional contour was formed on the screen.

Figure 4 shows photographs of the image obtained in the absence and in the presence of voltage supplied to the converter. In Fig. 4b, a well-defined two-dimensional contour is visible. Some structure is also seen inside the contour, indicating the presence of inhomogeneities in the intensity distribution of the initial radiation. Anyhow, in our opinion, there is good agreement between theory and experiment: the theoretically predicted two-dimensional contour at a low acoustic frequency (Fig. 3b) corresponds to the contour formed in the experiment (Fig. 4b). The results significantly expand the capabilities of AO diffraction for processing two-dimensional optical images.

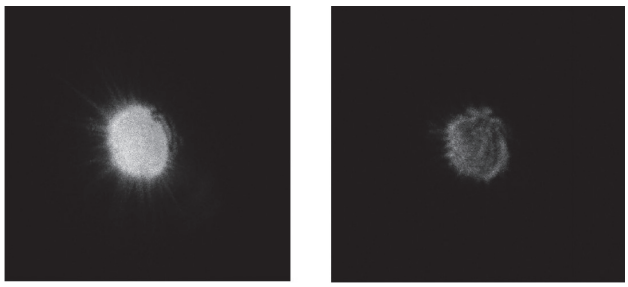

a b

Figure 4. Experimental Fourier image processing: (a) image without processing and (b) after processing.

4. Conclusions

Based on the presented results, we can make the following conclusions:

1. For two-dimensional image edge enhancement, it is proposed to use an AO spatial frequency filter based on two orders of Bragg diffraction, +1 and –1.

2. The transfer functions for the diffraction orders are found. For two-dimensional image filtering, it is proposed to use the transfer function corresponding to the zero Bragg order.

3. It is shown that the considered diffraction regime allows processing optical images in a wide band of acoustic frequencies. In particular, the frequency band in which a two-dimensional contour of an optical image is formed by radiation at a wavelength of 0.63 μm extends from ∼25 to 50 MHz.

4. The two-dimensional edge enhancement of an image carried by the optical radiation with a wavelength of 0.63 μm was obtained experimentally by optical Fourier processing using an AO spatial filter made of paratellurite operating at an acoustic frequency of 29 MHz.

The presented results can be used for processing optical images using an AO cell as a spatial frequency filter.

Acknowledgements. This work was carried out as part of a State Assignment on the topic No. 0030-2019-0014, as well as was partially supported by the Russian Foundation for Basic Research (Grant No. 19-07-00071).

References

1. Balakshy V.I., Parygin V.N., Chirkov L.E. *Fizicheskiye osnovy akustooptiki* (Physical Foundations of Acousto-Optics) (Moscow: Radio i svyaz', 1985).
2. Xu J., Stroud R. *Acousto-Optic Devices: Principles, Design, and Applications* (New York: John Wiley & Sons Inc., 1992).
3. Alippi A., Palma L., Socino C. *Appl. Phys. Lett*., **26** (7), 360 (1975).
4. Balakshy V.I., Galanova I.Yu., Parygin V.N. *Sov. J. Quantum Electron.*, **9** (5), 569 (1979) [*Kvantovaya Elektron*., **6** (5), 965 (1979)].
5. Balakshy V.I. *Radiotekh. Elektron*., **29** (8), 1610 (1984).
6. Athale R.A., van der Gracht J., Prather D.W., Mait J.N. *Appl. Opt*., **4** (2), 276 (1995).
7. Cao D., Banerjee P.P., Poon T.-Ch. *Appl. Opt*., **37** (14), 3007 (1998).
8. Kotov V.M., Shkerdin G.N., Shkerdin D.G., Kotov E.V. *J. Commun. Technol. Electron.*, **56** (1), 52 (2011) [*Radiotekh. Elektron.*, **56** (1), 66 (2011)].
9. Balakshy V.I., Voloshinov V.B. *Quantum Electron.*, **35** (1), 90 (2005) [*Kvantovaya Elektron*., **35** (1), 90 (2005)].
10. Balakshy V.I., Voloshinov V.B., Babkina T.M., Kostyuk D.E. *J. Mod. Opt*., **52**, 1 (2005).
11. Balakshy V.I., Kostyuk D.E. *Appl. Opt*., **48**, C24 (2009).
12. Kotov V.M., Shkerdin G.N., Bulyuk A.N. *Quantum Electron.*, **41** (12), 1113 (2011) [*Kvantovaya Elektron.*, **41** (12), 1113 (2011)].
13. Kotov V.M., Shkerdin G.N., Averin S.V. *Radiotekh.*, **12**, 57 (2012).
14. Kotov V.M., Shkerdin G.N. *J. Commun. Technol. Electron*., **58** (10), 1011 (2013) [*Radiotekh. Elektron*., **58** (10), 1040 (2013)].
15. Kotov V.M., Shkerdin G.N., Averin S.V. *J. Commun. Technol. Electron.*, **61** (11), 1275 (2016) [*Radiotekh. Elektron*., **61** (11), 1090 (2016)].
16. Voloshinov V.B. *Opt. Eng*., **31** (10), 2089 (1992).
17. Kotov V.M. *Opt. Spektrosk*., **77** (3), 493 (1994).
18. Shaskol'skaya M.P. (Ed.) *Akusticheskie kristally* (Acoustic Crystals) (Moscow: Nauka, 1982).
19. Kizel' V.A., Burkov V.I. *Girotropiya kristallov* (Gyrotropy of Crystals) (Moscow: Nauka, 1980).
20. Gonzalez R., Woods R., Eddins S. *Digital Image Processing Using MATLAB*, 2-nd Edition (Gatesmark Publishing, 2009).
21. Kotov V.M., Averin S.V., Kuznetsov P.I., Kotov Ye.V. *Quantum Electron*., **47** (7), 665 (2017) [*Kvantovaya Elektron*., **47** (7), 665 (2017)].
22. Kotov V.M., Averin S.V., Kotov E.V., Shkerdin G.N. *Appl. Opt*., **57** (10), C83 (2018).
23. Kotov V.M., Averin S.V., Kuznetsov P.I., Kotov E.V. *Opt. Zh*., **85** (1), 34 (2018).
24. Kostyuk D.E. *PhD Thesis* (Moscow, Lomonosov Moscow State University, 2008).